NREL
NATIONAL RENEWABLE ENERGY LABORATORY

Temperature-Dependent Measurements of an Inverted Metamorphic Multijunction (IMM) Solar Cell

Preprint

Myles A. Steiner, John F. Geisz,
Daniel J. Friedman, Waldo J. Olavarria,
Anna Duda, and Tom E. Moriarty

Presented at the 37th IEEE Photovoltaic Specialists Conference (PVSC 37)
Seattle, Washington
June 19-24, 2011

Conference Paper
NREL/CP-5200-50736
July 2011

Contract No. DE-AC36-08GO28308

NOTICE

Available electronically at http://www.osti.gov/bridge

Available for a processing fee to U.S. Department of Energy
and its contractors, in paper, from:

U.S. Department of Energy
Office of Scientific and Technical Information

P.O. Box 62
Oak Ridge, TN 37831-0062
phone: 865.576.8401
fax: 865.576.5728
email: mailto:reports@adonis.osti.gov

Available for sale to the public, in paper, from:

U.S. Department of Commerce
National Technical Information Service
5285 Port Royal Road
Springfield, VA 22161
phone: 800.553.6847
fax: 703.605.6900
email: orders@ntis.fedworld.gov
online ordering: http://www.ntis.gov/help/ordermethods.aspx

Cover Photos: (left to right) PIX 16416, PIX 17423, PIX 16560, PIX 17613, PIX 17436, PIX 17721

Printed on paper containing at least 50% wastepaper, including 10% post consumer waste.

TEMPERATURE-DEPENDENT MEASUREMENTS OF AN INVERTED METAMORPHIC MULTIJUNCTION (IMM) SOLAR CELL

Myles A. Steiner, John F. Geisz, Daniel J. Friedman, Waldo J. Olavarria, Anna Duda, and Tom E. Moriarty
National Renewable Energy Laboratory, Golden, CO 80401, USA

ABSTRACT

The inverted metamorphic multijunction (IMM) solar cell has demonstrated efficiencies as high as 40.8% at 25°C and 326 suns concentration. The actual operating temperature in a commercial module, however, is likely to be as much as 50-70°C hotter, reaching as high as 100°C. In order to be able to evaluate the cell performance under these real-world operating conditions, we have measured the open-circuit voltage, short-circuit current density and efficiency at temperatures up to 125°C and concentrations up to 1000 suns, as well as the temperature coefficients of these parameters. Spectral response and one-sun current-voltage characteristics were measured by carefully adjusting the incident spectrum to selectively current-limit the different subcells. Concentrator measurements were taken on a pulsed solar simulator to minimize any additional heating due to the high intensity illumination. We compare our measured values to predictions based on detailed models of various triple junction solar cells. By choosing the optimum bandgaps for high temperature operation, the IMM can potentially result in greater energy production and lower temperature sensitivity under real operating conditions than a Ge-based solar cell.

INTRODUCTION

The operating temperature of a solar cell is an important parameter for determining the conversion efficiency. Multijunction concentrator solar cells are typically evaluated under flash illumination at 25°C, but this standard measurement condition significantly underestimates the thermal load on the cell in an actual real-world module, where the steady-state concentrated illumination can raise the operating temperature to as high as 100°C. At elevated temperatures, the bandgaps of the subcells decrease which generally increases the photocurrent. At the same time, the open-circuit voltage (V_{oc}) and the efficiency generally decrease. To maximize the efficiency under realistic temperatures, the bandgaps of the subcells should ideally be chosen based on modeling at those temperatures. The inverted metamorphic multijunction (IMM) solar cell has allowed designers to fabricate high-efficiency solar cells with bandgaps that approach the ideal combination, and laboratory prototypes have demonstrated efficiencies as high as 40.8% at 25°C and 326X [1,2]. Several companies are presently developing commercial versions of the IMM. Because of the freedom to choose the bottom subcell bandgap, the IMM has the capability, in principle, of increasing the energy production under real operating conditions compared to Ge-based cells. Outdoor temperature measurements on lattice-matched Ge-based cells have been reported at both the cell level [3] and module level [4], and initial temperature-dependent results on aspects of epitaxial liftoff IMM cells were reported recently [5], but the efficiency of an IMM cell under controlled conditions at elevated temperature and concentration has not been fully investigated. In this paper, we report on measurements of the conversion efficiency of a triple junction IMM solar cell at temperatures up to 125 °C and concentrations up to 1000 suns. The cell studied here has bandgaps of {1.81, 1.40, 1.00} eV and was described in detail in reference [1]. This combination is close to ideal at 25°C under the G173 direct spectrum when the top two junctions are constrained to be lattice-matched $Ga_{.51}In_{.49}P$ and GaAs.

EXPERIMENT

The inverted structures were grown at NREL in an atmospheric pressure OMVPE reactor, and processed using standard cleanroom lithographic techniques applied to an inverted device [1,2]. The structure is grown with the top two subcells lattice-matched to the GaAs substrate, and with the top subcell thinned to 1 μm to try to match the photocurrent of the middle subcell. A transparent GaInP graded buffer then reduces the in-plane lattice constant to create a virtual substrate for the GaInAs bottom subcell. During processing, the structure was bonded to a silicon wafer handle and the original GaAs substrate removed. A bilayer ZnS/MgF_2 anti-reflection coating was deposited after fabrication. Cells were processed with a mesa area of 0.12 cm^2 and an illuminated area of 0.10 cm^2. Numerous such cells have been fabricated at NREL and were screened at one-sun to find high-performing devices. Single junction isotype cells corresponding to the three subcells were also fabricated and measured. The isotype cell for a given subcell has the same structure in the active layer as the subcell and nominally the same filtering layers above but without p-n junctions.

To control the temperature during all measurements, a gold-plated copper sample stage was mounted on a thermoelectric heater, powered by a Wavelength Electronics LFI-3751 controller. Temperature was monitored with a 10 kΩ thermistor that was embedded in the copper block, and the surface temperature was measured with a calibrated platinum-RTD surface probe. Data were collected at nominal ambient temperatures of 25, 53, 85, 105 and 126 °C as determined by the surface probe. Temperatures were adjusted to within 0.5° on the various instruments.

Cells were carefully measured at different temperatures as follows: the spectral response of each subcell (and

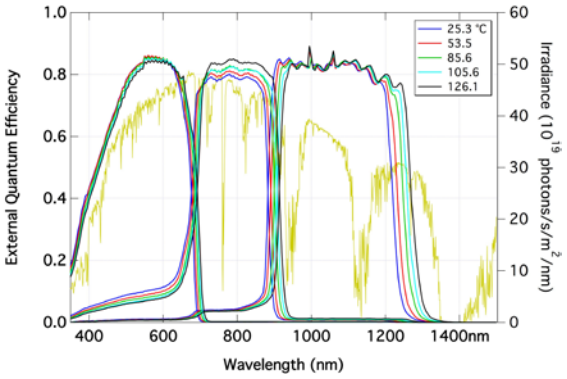

Figure 1 External quantum efficiency as a function of ambient temperature. The bandgaps at 25°C are 1.81, 1.40 and 1.00 eV. The yellow curve is the G173 direct spectrum at 1000 W/m^2.

isotype) was measured at each temperature and then used in conjunction with calibrated reference cells to appropriately adjust the spectrum on a solar simulator. The simulator spectrum had to be re-adjusted for each temperature before the one-sun IV curves could be measured, and care was taken to regain the same temperature under the simulator as during the QE measurement. Note that the reference cells remained at 25°C. Cells were then measured at high concentration under a flash simulator with the spectrum adjusted as much as possible for each temperature, and the concentrations were calculated using the one-sun short-circuit current density for the appropriate temperature. We assume that the subcell photocurrent ratios at any particular temperature remain constant with concentration.

The experimental procedure outlined here ensures (as much as possible) that the observed temperature dependences of the V_{oc}, J_{sc}, FF and efficiency reflect the interaction of the cell with the features of the reference spectrum rather than with the particular characteristics and idiosyncrasies of the simulator spectrum. This is especially true for Xenon-lamp-based simulators with strong emission peaks, though it also remains true for newer metal-halide-based simulators, for example [5]. Outdoor on-sun measurements can obviously come quite close to achieving the correct spectrum, though the air mass can vary widely over the course of the day, and taking measurements at high concentration requires special attention to the spectral effects and uniformity of the particular optics.

External quantum efficiency (EQE) measurements were taken with a combination of light-biasing and voltage-biasing, to properly measure the individual subcell QEs; LEDs at 465, 850 and 940 nm were used for the light-biasing. One-sun current-voltage (JV) measurements were taken on a Spectrolab X25 multisource simulator. The single junction isotype cells were measured on a single source simulator.

The one-sun JV curves for the IMM were also measured separately on a single-source simulator with additional high-power collimated LED biasing lights, to selectively current-limit each of the junctions and measure the subcell JV curves. The limiting subcell was always

subcell	d(E_g)/dT (meV/°C)	d(J_{sc})/dT (μA/cm^2/°C)	d(V_{oc})/dT (mV/°C)
GaInP	-0.43	7.1 ± 0.5	-2.21 ± 0.04
GaAs	-0.47	-2.8 ± 0.9	-2.27 ± 0.04
GaInAs	-0.40	--	-2.06 ± 0.04
IMM	N/A	5.3 ± 0.6	-6.44 ± 0.07

Table 1 One-sun temperature coefficients of E_g, J_{sc} and V_{oc} for the IMM subcells. The V_{oc} coefficients are derived from matched isotypes. Uncertainties on the E_g coefficients are ± 0.02. The bottom row lists the coefficients of the full triple junction as derived from the X25 multisource measurements.

illuminated at nominally one-sun as determined by a matched set of calibrated reference cells, and the two other junctions were over-illuminated with LED light. Three separate curves are required at each temperature, limiting each of the top, middle and bottom junctions, and the total spectrum was determined for each illumination condition. The analysis of the data follows the general method of Kurtz *et al.* [6], with additional corrections for spectral mismatch between the temperature-dependent EQE of the device and the 25°C EQE of the reference cells.

Concentrator measurements were taken on a Spectrolab pulsed solar simulator (HIPSS), where the lamp voltage was adjusted at each temperature to obtain the correct photocurrent ratio between the GaInP and GaAs subcells, based on the EQE. Raising the lamp voltage increases the spectral content in the UV range and damps out the spikes observed in the spectrum in the near-IR region. The intensity was controlled with a pair of apertures near the flash bulbs. With only one adjustable control on the flash spectrum, precise matching of the photocurrent ratios between all three subcells is impossible, but we estimate the illumination of the bottom subcell to be ≤ 5% high, and the one-sun data indicate that the bottom subcell was never current-limiting.

RESULTS

Figure 1 shows the EQE measured at five temperatures. Each subcell plateaus at approximately 85% which includes a 6.7% shadow loss from the grid coverage and a ~3-5% reflection loss. The plateaus remain approximately constant as temperature increases, but the bandgap of each subcell decreases linearly with temperature, consistent with the Varshni model in this temperature range. The coefficients are listed in Table 1. The short-wavelength tails on the middle subcell EQEs appear to be real rather than measurement artifacts, and do not decrease in magnitude with changes in light-biasing or voltage-biasing. We speculate that these tails result from photon coupling between the top and middle subcells [7]. We would expect the same effects to be present at short-circuit under a solar simulator, so the tails cannot be ignored when using the spectral response to adjust the simulator, as discussed below.

The short-circuit current densities (J_{sc}) at 1000 W/m^2, as measured on the single-source simulator with LED

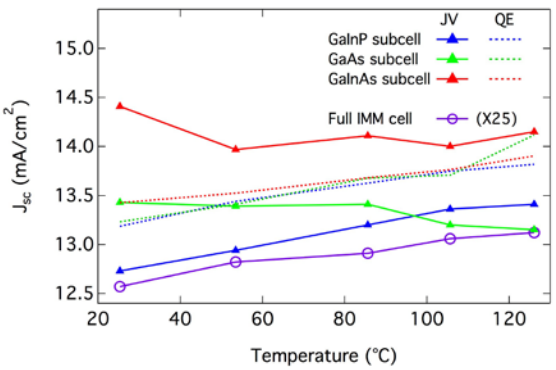

Figure 2 J_{sc}(T) for the IMM subcells. Solid lines were measured on a single source simulator using LED bias lights to over-illuminate the non-limiting junction. Dotted lines are based on the EQE. The purple curve (open circles) shows the J_{sc} values for the full IMM cell as measured on the X25 multisource simulator.

biasing, are shown in Figure 2 (solid triangles). J_{sc} for the GaInP subcell increases linearly with temperature at a rate of (7.1 ± 0.5) μA/cm^2/°C. The J_{sc}(T) dependences for the GaAs and GaInAs subcells are more complicated, as they depend on the bandgaps of both the subcell in question and of the subcell above, which filters the shorter wavelength light. They may also depend on the degree of photon coupling from the subcell above [7]. The GaAs J_{sc} decreases slightly with temperature while the GaInAs J_{sc} is approximately constant to within the noise in the data. The actual J_{sc}(T) for the multijunction follows the minimum of the subcell curves. As noted above, the short-wavelength tails on the GaAs subcell EQE likely represent the effect of photon coupling from the top subcell, and close inspection of Figure 1 shows that the tails decrease in magnitude with temperature. Given the significant spectral content in the 500-650 nm wavelength range, this represents a loss in J_{sc}(T) and helps explain why the overall GaAs subcell J_{sc} decreases. Indeed a GaAs isotype cell deliberately grown without the short-wavelength tail and measured in the same way shows a slight *increase* in J_{sc} with temperature.

J_{sc}(T) data from the one-sun X25 multisource measurement are also shown in Figure 2 as open circles. The data from the two simulators follow each other reasonably well, with a small offset. The X25 data correspond to a temperature coefficient for the IMM J_{sc} of d(J_{sc})/dT = (5.3 ± 0.6) μA/cm^2/°C at one sun.

The 1 μm top subcell thickness was chosen to match photocurrents with the GaAs subcell, but the calculation does not include the effects of photon coupling. Therefore the middle subcell produces extra photocurrent and the photocurrents are not matched at 25°C. Most significantly, the cell crosses over from top-cell limited at low temperature to middle-cell limited at high temperature. If the temperature were increased much above 126°C, the bandgap of the current-limiting GaAs subcell would cross into the prominent water absorption band at ~930 nm in the terrestrial spectrum, shown in Figure 1, and the total J_{sc} would decrease significantly.

Figure 2 also shows as dashed lines the J_{sc}s as calculated directly from the subcell EQEs of Figure 1, by integrating the product of (EQE x spectrum). It would appear from these latter data that J_{sc} for all three subcells increases linearly with temperature, and that the top and middle subcells remain closely current-matched until over 100°C. However, these curves are substantially offset from the purple X25 curve. Calculating J_{sc} in this way requires an absolute EQE measurement, often difficult to achieve and especially so for small cells and for cells where there is any significant shunt conductance on any of the subcells, as in the case of the GaAs subcell in the IMM measured here. The EQE for a multijunction cell is also difficult to measure under one-sun illumination and was measured here at much lower intensities, which may introduce errors if J_{sc} is not strictly linear with intensity at low intensities. The calculated J_{sc}s are therefore directly affected by any error in the EQE. By contrast, measuring the subcell J_{sc}s by selectively light-biasing the various subcells under the solar simulator as described here is a technique that is based on using primary-calibration reference cells to accurately set the intensity. Spectral effects are subsumed into a spectral mismatch correction factor that is immune from absolute errors in the EQE [8], and any spectral errors in the EQE (ie. shape) are shifted to a higher-order correction.

One-sun JV curves for the three single junction isotypes were also measured as a function of temperature to find the temperature coefficients of V_{oc}, listed in Table 1. The values are consistent with those reported in the literature [5,9]. One expects the voltage coefficient of the multijunction cell to be the sum of the voltage coefficients of the individual subcells. Here the individual coefficients sum to (-6.54 ± 0.07) mV/°C which agrees with the value of (-6.44 ± 0.07) derived from the X25 multisource measurement.

High concentration JV curves were measured on the HIPSS and normalized by the one-sun J_{sc} values from the X25 measurement. The characteristics of these data are plotted in Figure 3 as a function of concentration. The top panel shows the expected logarithmic dependence of V_{oc} on concentration over the full temperature range. There is some roll-off observed above ~700 suns which we tentatively attribute to heating, because the cell is secured to a silicon wafer with a 10 μm thin, thermally insulating epoxy; further investigation is underway to confirm this. Since commercial production versions of the IMM are generally designed to be well-heat-sunk using thermally conductive epoxies or solders, or wafer-bonding processes, the roll-off observed here is not expected to be reproduced in production cells.

For a given concentration, the V_{oc} decreases linearly with temperature, and calculating dV_{oc}/dT at each concentration gives the thermal coefficient of V_{oc} at various concentrations, shown in Figure 4. The general trend of dV_{oc}/dT with concentration is consistent with modeling. dV_{oc}/dT decreases from -6.4 mV/°C at one sun to -4.0 mV/°C at 1000 suns, as expected [10].

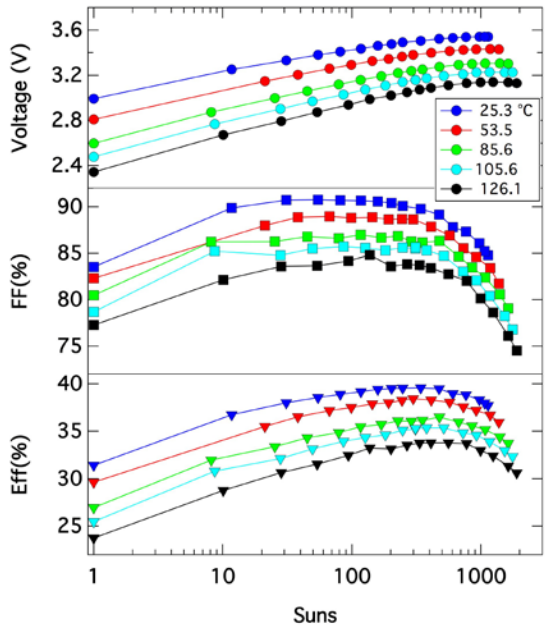

Figure 3 Solar cell parameters extracted from the HIPSS data. The one-sun values were measured separately and used to normalize the concentration axis. The illuminated cell area was 0.1 cm^2.

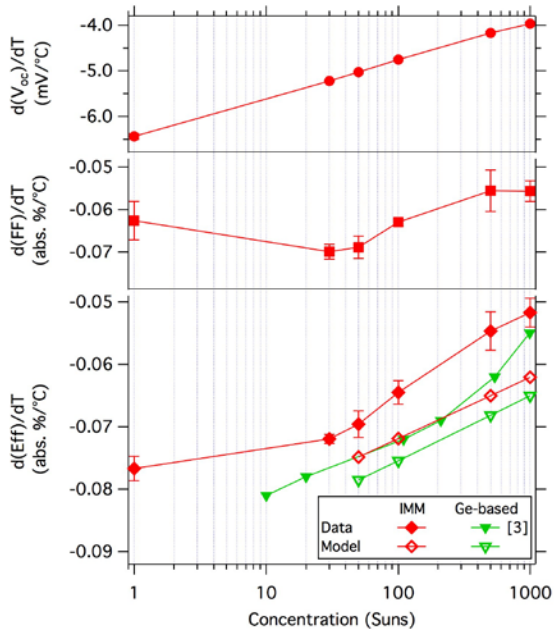

Figure 4 Temperature coefficients of V_{oc}, FF and efficiency as a function of concentration. The green curves in the bottom frame show results for a Ge-based triple junction, from ref [3]. Open symbols show modeled results for the IMM and the Ge-based cell.

The middle panel of Figure 3 shows the fill factor as a function of concentration; the one-sun values are from the X25 measurement. The FF rises nearly linearly from one sun to ~100 suns before beginning to roll over. This near-linearity in FF with Log(concentration) at all temperatures indicates that the spectrum was accurately adjusted: for high quality solar cells under a fixed spectrum, the FF is expected to increase linearly with Log(Concentration), before resistive effects begin to dominate. At the same time, for multijunction solar cells the fill factor is always minimized when the subcell photocurrents are matched [11]. Assuming the one-sun FF is correct for a particular temperature, large misadjustments in the HIPSS spectrum would therefore tend to inflate the FF of the concentrated IV curves, and one would expect to see a large jump in FF from one-sun to several suns rather than a smooth increase.

The FF decreases with increasing temperature, but more slowly at higher concentrations, as indicated in Figure 4. The FF peaks at higher concentrations as the temperature increases. This latter trend is also clearly visible in the bottom panel of Figure 3, showing the efficiency as a function of concentration: the efficiency peak increases from 290 suns at 25°C to 460 suns at 126°C; the peak efficiency correspondingly drops from 39.5% to 33.8%.

The increase in peak concentration is possibly the result, in part, of enhanced thermionic emission over one or more of the various heterojunction interfaces between junction layers and confinement layers within the device, effectively lowering the resistive barrier to majority carrier transport [12]. In addition to the emitter sheet resistance, these internal resistances all contribute to efficiency rollovers at several hundred suns rather than several thousand. These internal resistances are the subject of ongoing experimental and theoretical investigations.

The efficiency data show a linear decrease in efficiency with increasing temperature. The temperature coefficients at various concentrations are also shown in Figure 4. The IMM is less sensitive to temperature variations at higher concentrations, varying by -0.052 %/°C at 1000 suns compared to -0.077 %/°C at one-sun. Taking 500X and 75°C as representative of a typical concentrator module, and comparing the performance to 500X and 25°C, the conversion efficiency of this particular IMM cell decreases from 39.6% to 36.8%, a relative change of about eight percent.

DISCUSSION

The IMM design need not have only one lattice-mismatched junction. The triple-junction cell in reference [2] that demonstrated 40.8% efficiency had mismatched bottom *and* middle cells. The IMM presents a platform for exploring various bandgap combinations, some of which may be more appropriate for a cell that is meant to operate at elevated temperatures rather than at 25°C. Figure 5 shows the modeled dependence of cell efficiency on temperature for several different combinations of junction bandgaps, at 500 suns. The calculation uses a dark current model which aims to more realistically match the magnitudes of the dark currents to what is experimentally achievable than does the detailed-balance approach [13], while maintaining the proper temperature dependence [14]; in the detailed-balance approach, the efficiencies of Figure 5 would be several points higher

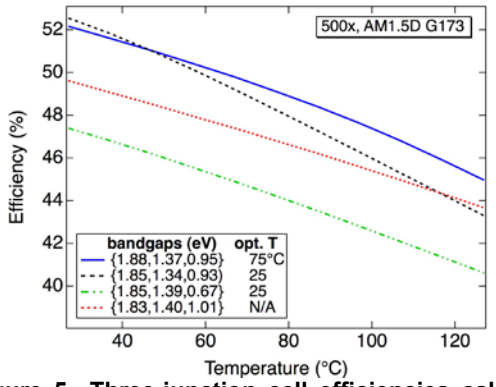

Figure 5 Three-junction cell efficiencies calculated for several different combinations of junction bandgaps, as a function of cell operating temperature. The cells are illuminated by the G173 AM1.5 direct spectrum at 500 suns. In cases where the bandgap combination has been optimized for a given cell operating temperature, that temperature is indicated in the figure legend. The indicated bandgaps are all at 25°C; for cell operating temperatures other than 25°C, the model accounts for the change of bandgaps with cell temperature.

because the calculation does not account for as many loss mechanisms, but the overall trends would be the same as shown.

The {1.81, 1.40, 1.00} eV bandgap combination corresponding to the cell studied here is represented by the red dotted line in Figure 5. Modeling by Kurtz *et al.* [15] showed that a ~1.0 eV third junction would maximize the 25°C, 500X efficiency of a triple junction with fixed $Ga_{.51}In_{.49}P$ and GaAs upper subcells. This represents the simplest IMM design, with only one mismatched junction, but Figure 5 clearly shows other bandgap combinations that realize increased conversion efficiencies. The {1.85, 1.34, 0.93} eV combination is optimal for a 25°C (~300K) operating temperature, while for a 75°C (~350K) operating temperature, higher bandgaps of {1.88, 1.37, 0.95} eV are optimal. For both cases there is also a second local maximum in efficiency corresponding to bandgap combinations with bottom junction bandgaps of around 0.7 eV which give comparable efficiencies [14]; here we focus on the designs with the higher ~0.93-0.95 eV bottom junction bandgap, which in the InGaAs materials system is more closely lattice-matched to GaAs. The design which is optimized for 75°C is only slightly sub-optimal at 25°C, while being significantly better than the 25°C design at 75°C and above. For comparison, the figure also shows the efficiency curve for the {1.85, 1.39, 0.67} eV bandgap combination of the industry-standard GaInP/Ga(In)As/Ge cell, which was designed to be lattice-matched to a Ge substrate for ease and cost-effectiveness of production.

The 75°C optimal cell design is similar to the IMM cell in reference [2] with two mismatched junctions, at 1.34 eV and 0.89 eV, but the optimal design requires less-severe graded buffers for both the middle and bottom junctions, and a slightly elevated top subcell bandgap.

The modeled temperature dependences can be compared with experimental data where available. We calculated d(Eff)/dT for the {1.81, 1.40, 1.00} eV cell at 500X from Figure 5 and repeated the modeling at 50, 100 and 1000X. The calculated coefficients are plotted in the bottom frame of Figure 4 (open diamonds). The values are slightly greater than the experimental data but the dependence on concentration is approximately the same. Figure 4 also includes experimental data from Kinsey *et al.* [3] on the Ge-based triple junctions, as well as modeled results for that bandgap combination. Both the experimental data and the simulated results show a lower sensitivity to temperature, at all concentrations, for the IMM cell studied here as compared to the Ge-based device.

It is worth commenting briefly on the effect on Eff(T) of the prominent water absorption band at 0.90 eV (~1377 nm) in the terrestrial spectrum, shown in yellow in Figure 1. Highest efficiency at 75°C is achieved by having optically thick junctions with a bottom subcell bandgap energy just above the absorption band, so that the photon collection is maximized. In an unfiltered single junction cell, the photocurrent would simply plateau as the bandgap decreases into the absorption band at elevated temperatures, but in a multijunction cell the bandgap of the filtering middle junction also decreases with temperature, and therefore the photocurrent generated by the bottom subcell will drop sharply with temperature. The bottom subcell may even become current-limiting at some temperature, with a corresponding decrease in efficiency. It is therefore deleterious to design a cell such that the bottom subcell bandgap is situated in the water absorption band at the expected operating temperature. One may note that the bandgap combination designed for 25°C operation has a 0.93 eV bottom subcell, just above the water absorption band, whereas the cell designed for 75°C has a 0.95 eV bottom subcell *as measured at room temperature*. We observed in Figure 1 that the bandgap of the GaInAs bottom subcell shifts to longer wavelengths, changing by -0.40 meV/°C. Based on this shift, we predict that at 75°C the 0.95 eV cell will have a bottom subcell bandgap shifted to 0.95 eV – 0.40 meV/°C x 50°C = 0.93 eV, again optimally positioned just above the water absorption band.

In summary, we have conducted a careful measurement of the performance of a {1.81, 1.40, 1.00} eV IMM solar cell as a function of temperature and concentration. The measurement involves a complete data set of spectral response, one-sun JV and concentrator JV for each temperature. The peak efficiency decreases from 39.5% at 290 suns and 25°C to 33.8% at 460 suns and 126°C. $J_{sc}(T)$ of the individual subcells can also be measured and indicate a crossover from top-cell-limited to middle-cell-limited behavior at ~100°C.

ACKNOWLEDGEMENTS

The authors thank M. Young for dedicated work fabricating the cells, and J. Olson, R. France, P. Ciszek and C. Osterwald for useful conversations. Work was supported by the U.S. Department of Energy under Contract No. DE-AC36-08GO28308 with the National Renewable Energy Laboratory. This work is subject to government rights.

REFERENCES

[1] J.F. Geisz *et al.*, "High-efficiency GaInP/GaAs/InGaAs triple-junction solar cells grown inverted with a metamorphic bottom junction," *Appl. Phys. Lett.* **91**, 2007, p. 023502.

[2] J.F. Geisz *et al.*, "40.8% efficient inverted triple-junction solar cell with two independently metamorphic junctions," *Appl. Phys. Lett.* **93**, 2008, p. 123505.

[3] G.S. Kinsey *et al.*, "Concentrator multijunction solar cell characteristics under variable intensity and temperature," *Prog. Photovolt: Res. Appl.*, **16**, 2008 pp. 503–508.

[4] G. Peharz *et al.*, "Investigations on the temperature dependence of CPV modules equipped with triple-junction solar cells," *Prog. Photovolt: Res. Appl.*, **19**, 2011 pp. 54–60.

[5] R. Tatavarti *et al.*, "Temperature dependent measurements of inverted metamorphic (IMM) ELO solar cells," poster presented at CPV-7, 2011.

[6] S.R. Kurtz, K. Emery and J.M. Olson, "Methods for analysis of two-junction, two-terminal photovoltaic devices," *1st WCPEC*, 1994, p. 1733.

[7] Carsten Baur *et al.*, "Effects of optical coupling in III-V multilayer systems," *Appl. Phys. Lett.* **90**, 2007, p. 192109.

[8] C.R. Osterwald, "Translation of device performance measurements to reference conditions," *Solar Cells* **18**, 1986, pp.269–279.

[9] Liu Lei *et al.*, "Quantum efficiency and temperature coefficients of GaInP/GaAs dual-junction solar cell," *Sci. China Ser. E-Tech Sci.,* **52**, 2009, pp. 1176–1180.

[10] D.J. Friedman, "Modelling of tandem cell temperature coefficients," *Twenty-fifth IEEE PVSC*, 1996, p. 89.

[11] W.E. McMahon *et al.*, "Fill factor as a probe of current-matching for $GaInP_2$/GaAs tandem cells in a concentrator system during outdoor operation," *Prog. Photovolt: Res. Appl.*, **16**, 2008, pp. 213–224.

[12] J. Olson, M.A. Steiner, A. Kanevce, "Using measurements of fill factor at high irradiance to deduce heterobarrier offsets," *Thirty-seventh IEEE PVSC*, 2011.

[13] W. Shockley and H.J. Queisser, "Detailed balance limit of efficiency of p-n junction solar cells", *J. Appl. Phys.* **32**, 1961, pp. 510—519.

[14] D.J. Friedman, "Progress and challenges for next-generation high-efficiency multijunction solar cells", *Curr. Opin. Solid State Mater. Sci.* **14**, 2010, pp. 131–138.

[15] S.R. Kurtz, D. Myers, and J.M. Olson, "Projected Performance of Three- and Four-Junction Devices Using GaAs and GaInP," *Twenty-sixth IEEE PVSC*, 1997, p. 875.